Erosional forcing of basin dynamics: new aspects of syn- and post-rift evolution

E. BUROV[1] & A. POLIAKOV[2]

[1]*University of Pierre et Marie Curie, Paris, France*
[2]*CNRS/University Montpellier II, Montpellier, France*

Abstract: We revisit a number of important topics associated with the problem of interactions between surface and subsurface processes during syn- and post-rift evolution. To demonstrate the importance of these interactions and to verify a number of earlier ideas on rift evolution, we use a fully coupled three-fold mechanical behaviour, surface processes, heat transport numerical model, which combines brittle-elastic-ductile rheology, fault localization, erosion and sedimentation mechanisms. The model simulates fault formation causing brittle strain localization. Fault distribution and evolution are thus outputs of the model, allowing for new, geologically sensible constraints on the results. The numerical algorithm accounts for 'true' surface erosion/sedimentation, that is, the numerical elements are eliminated (eroded) and created (sedimented) with respective changes in properties. The results show that sedimentation in the basin and erosion on the rift flanks strongly control the mode of extension. In particular, active erosion/sedimentation on the synrift phase results in more pronounced thinning and widening of the basin, so that the apparent coefficients of extension increase by a factor of 1.5–2. Surface loading/unloading results in lithospheric flexure. Flexural stresses in places of maximum bending exceed lithospheric strength and create zones of localized weakening that partly or completely compensate strengthening due to cooling in the post-rift phase, when the subsidence rates also accelerate. Erosional unloading on the rift shoulders has the opposite effect, producing local strengthening and flexural rebound. Pressure gradients induced by subsidence/rebound result in lower crustal flow that controls 20–30% of subsidence rates, stability of the rift shoulders and drives some post-rift extension or compression. By taking account for the intermediate and lower crustal rheology, new explanations for some synrift phase effects such as polyphase subsidence of the basement provoked by crustal flow and 'switching' of the level of necking from one competent lithospheric level to another are suggested. Syn- and post-rift stagnation, upward and downward accelerations find a natural explanation within our model without the necessity to invoke external mechanisms.

The majority of present-day models of continental rifting do not associate mechanisms of rift necking and subsidence with syn- and post-rift surface processes (sedimentation, surface transport and erosion). Some workers demonstrate the importance of a number of secondary effects of sedimentation such as retarded cooling due to heat screening by sediments with low thermal conductivity (Stephenson *et al.* 1989; England & Richardson 1980). Others account for simplified elastic flexural response to surface loading/unloading by erosion and sedimentation (Kooi & Beaumont 1994; Balen *et al.* 1995). Finally, Burov & Cloetingh (1997) considered the influence of surface processes on basin evolution using a rheologically realistic semi-analytical model, yet limited to consideration of the post-rifting phase and neglecting faulting. Poliakov *et al.* (in press) conducted a complementary study accounting for synrift erosion, but also using a continuous (no faulting) analytical model with highly simplified rheology and erosion laws.

Formation and maintenance of rift flank escarpments was explained by different mechanisms: lateral heat transport and associated thermoelastic effects, variation in horizontal and vertical forces associated with the far-field regime and lithosphere-asthenosphere interactions, phase changes, flexural forces, small-scale convection, underplating (e.g. Cloetingh *et al.* 1982; Braun & Beaumont 1989; Beaumont *et al.* 1992; Chéry *et al.* 1992; Kusznir & Karner 1985; White & McKenzie 1988; Kusznir 1991; Watts & Torne 1992; Bassi 1995; Cloetingh & Burov 1996). However, previous studies do not account for the fact that for sufficiently deep basins, evolution of the rift must be influenced by production and lateral redistribution of important amounts of normal surface load (Burov & Cloetingh 1997). The sedimen-

From: NIEUWLAND, D. A. (ed.) *New Insights into Structural Interpretation and Modelling*. Geological Society, London, Special Publications, **212**, 209–223. 0305-8719/03/$15

tation and surface denudation result in hundreds of megapascals of temporal and lateral variations of over burden stress and thus are as important as any other tectonic forces acting on the rift system. Erosion is faster on elevated topography and steep slopes (gravity-driven surface processes, wind and physical weathering) and on newly created topography (chemical and all types of climate weathering: van der Beek *et al.* 1995; van Balen *et al.* 1995; Burov & Cloetingh 1997). Gravity drives short-range land-sliding and long-range fluvial transport that carry eroded material from high relief to low relief areas. Consequently, the uplift on the flanks and subsidence in the basin are interlinked not only via tectonic mechanisms but also via surface processes. Erosion on the rift flanks controls sedimentary load accumulated in the basin. In most continental rift zones, loading and unloading of the crust by erosion is equivalent to the surface load created by mountain ranges (5–10 km of sediments, e.g. Pannonian basin, Albert rift, Baikal rift). This allows us to suggest that erosional unloading and sedimentary loading are as important as the other mechanisms controlling basin dynamics. Surface process-related loads may weaken the lithosphere via: (1) faulting in the brittle part; (2) flow in the ductile parts (Fig. 1b; see also Lobkovsky & Kerchman 1992; Hopper & Buck 1996); (3) erosional thinning of the uppermost strong brittle crustal layers followed by their isostatic replacement by weak ductile material coming from beneath (Fig. 1a). Burov & Cloetingh (1997) already suggested that this should result in more localized loading in the central parts of the basin, enhanced extension and maintenance of high strength closer to the flanks. This idea is supported by a number of recent field studies (e.g. Ebinger *et al.* 1989, 1999). As known from rock mechanics studies, the lithosphere behaves as a *de facto* elastic-plastic-ductile medium (e.g. Ranalli 1995). Its rheology is far more complex than the linear elastic or viscous rheology assumed in most previous basin models. One of the main properties of the lithospheric rheology, which differs from commonly inferred linear models, is a possibility to change the mechanical behaviour from elastic to brittle or ductile when the deformational stress exceeds depth-specific pressure- and temperature-controlled yield stress limits. This results in strong mechanical weakening of the material in zones affected by changes in the mechanical behaviour. The strongly non-linear properties of the stress-strain relationships characterizing the lithospheric rheology should influence the subsidence rates and subsidence phases known from tectonic geomorphology and fission-track age/length patterns (Rohrman *et al.* 1995).

Previous studies of interactions between surface and subsurface processes (Burov & Cloetingh 1997; Poliakov *et al.* in press) were focused on basin evolution-erosion interactions using continuous semi-analytic lithospheric models. In the present study, we numerically investigate the influence of surface processes on both syn- and post-rift evolution with primary emphasis on the interplay with faulting and ductile flow during the synrift phase. For this purpose we use a specially modified numerical code, Paravoz, originating from the algorithm used in the FLAC method (Cundall 1989), which allows for brittle and viscous strain localization and accounts for 'true' surface erosion. That is, the numerical elements are eliminated ('eroded') and created ('sedimented') with appropriate changes in physical properties.

Erosion and basin evolution: conceptual background

Erosion is a highly selective process. Inside the same system, the erosion rate may vary by several orders of magnitude. It is lowest on flat topography and fastest on steep, rough topography, such as forming rift flanks, and on crests of tilted blocks (Fig. 1). In isostatically balanced systems, unloading (erosion) of newly created topography results in compensatory rock uplift. At the surface, this uplift occurs at the expense of strong brittle upper crustal material removed by erosion and compensated by the ascent of the weak, ductile crustal material from below. Consequently, the mechanically competent part of the system vanishes without additional tectonic extension (Fig. 1). Such non-extensional thinning of the upper crust facilitates further regional extension. In the vicinity of the rift flanks, the crustal up-flow is predictably most intensive, because the ductile crust is squeezed from the centre to the flanks of the rift due to the increasing normal load (sediments) in the centre. This increase results from two mechanisms: (1) lithospheric necking, due to which the ductile crustal channel thins much faster in the centre than at the sides; (2) preferential growth of the surface load in the rift centre due to accumulation of sedimentary material. Consequently both tectonic and surface processes are linked by the isostatic response and lower crustal flow.

Basin subsidence is caused by three major factors: (1) crustal thinning on the synrift phase; (2) thermal cooling; and (3) sediment loading. Rifting results in thinning of the low viscosity lower crust, which may gradually restore its initial thickness in the post-rift phase. As expected, dynamic pressure differences created by erosion/sediment loading in the lower crust (10–50 MPa; Burov & Cloetingh 1997) can compensate other contributions to the non-hydrostatic pressure (Fig. 1). The pressure dif-

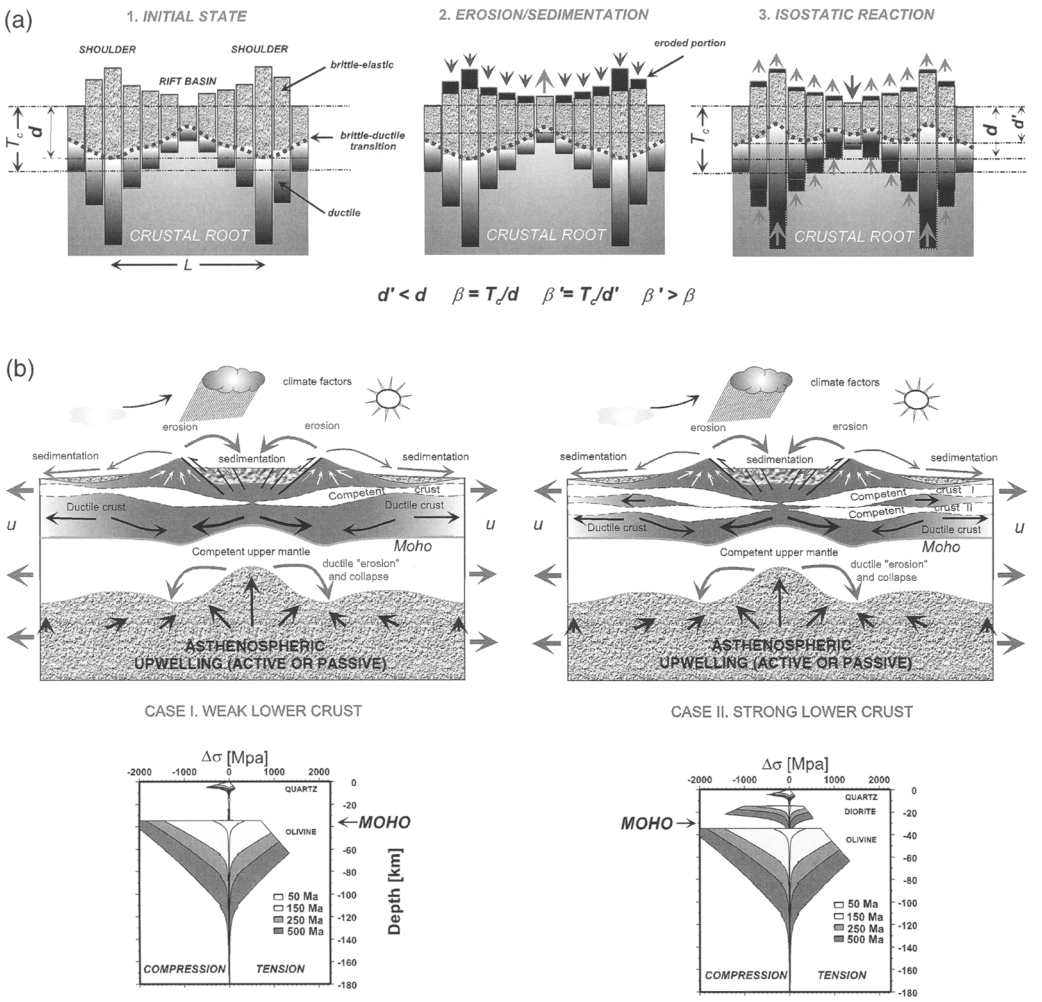

Fig. 1. (**a**) Simplified cartoon explaining weakening of the extended crust due to erosional removal and reworking of strong brittle parts with isostatic replacement by weaker ductile parts in the ideal case of local isostasy. L is the initial reference length, T_c is the normal crustal thickness, d is the thickness of the thinned crustal layer before erosion, d' is the thickness of this layer after erosion, β is the stretching factor before erosion, β' is the stretching factor after erosion. Note reduction of the thickness of the strong brittle portion of the upper crustal layer. (**b**) Set-up of the numerical problem. Sediments derived from erosion on slopes of rift shoulders result in increase of load in the basin. Strong parts of the crust and of the mantle lithosphere bend and weaken by flexural yielding (local reduction of the thickness of the competent cores). As a result, the integrated strength drops beneath the basin and shoulders (bottom) and becomes even lower than that immediately after extension. The lower crustal material flows from the centre of the basin towards the shoulders facilitating their uplift. The basic lithological structures are shown, one (left) with ductile intermediate and lower crust and another (right) with competent intermediate or lower crust resulting in appearance of a second competent and ductile crustal layer. The corresponding rheological yield-stress envelopes (yield stress as a function of the depth and thermotectonic age) are shown in the bottom of the figure. u is horizontal extension rate.

ference resulting from crustal flow is equal to $2\mu * \dot{\epsilon}$ where μ is the effective viscosity and $\dot{\epsilon}$ the strain rate. The flow stress must be equal to the ductile yield strength, which is 10 to 50 MPa in the lower crust (Burov & Cloetingh 1997). Let us assume a simple case of local isostasy considered in McKenzie (1978). Let us also assume some commonly inferred parameters: the initial total crustal thickness h_c = 30–40 km, subsidence rate $\Delta\nu$ = 1 mm a^{-1} (~3 × 10^{-11} m s^{-1}), and coefficient of exten-

sion $\beta = h_c/(h_c - \Delta w) = 2$. Here Δw is the value of crustal thinning. Based on these parameters, the depth-averaged vertical strain rate $\dot{\epsilon}_y = dv/dy$ will be on the order of 10^{-15} s^{-1} (dv/dy ranges from $(\Delta v + \Delta v \rho_m/\Delta\rho)/h_c$ to $(\Delta v + \Delta v \rho_m/\Delta\rho)/(h_c - \Delta w)$, where ρ_m is the density of the mantle and $\Delta\rho$ is the difference between the overlying material and that of the mantle; $\rho_m/\Delta\rho$ ranges from 3 to 5). Continuity and mass conservation require equivalent horizontal and vertical strain rates. Thus the associated horizontal strain rate in the ductile crust should be on the same order as the vertical strain rate. This conclusion could be a trivial matter if the subsidence was entirely caused by extension and thermal cooling of the whole lithosphere. Yet the presence of a weak ductile crust, which cannot always support extra sedimentary loading, may result in downward deflection of the crustal brittle-ductile boundary. This boundary will subside into the ductile crustal channel, which will force horizontal crustal outflow and thinning of the channel (Fig. 1b). The horizontal strain rate in the ductile crust must be the same as the vertical strain rate, with both rates depending on the viscosity of the lower crust. For example, strong lower crust means zero differential subsidence, whereas weak lower crust (i.e. viscosity of 10^{19} Pa s) means initiation of crustal flow already after deposition of several hundred metres of sediments.

In rheologically stratified lithosphere consisting of alternating weak and strong layers, the latter may be allowed to slip with respect to one another. The strain rates thus can vary with depth. The lower or intermediate crust is remarkably weaker than the upper crust and mantle, and the ductile crust thus can be thinned faster than the other layers (e.g. Royden & Keen 1980). For this reason, during the synrift phase basin subsidence can be primarily accommodated in the lower or intermediate crust (shallow level of necking), whereas the other lithospheric layers just bend down or upward preserving their initial thickness. Assuming that, we can conclude that the mean crustal β factor of 2 may associated with much higher lower crustal β factor (from 10 to 1000) and, consequently, with strain rates 5–500 times higher (10^{-14} to 10^{-13} s^{-1}) than the depth-averaged value for the whole crust. The associated flow stresses may exceed 50–100 MPa. The contribution of the ductile crustal flow in the observed subsidence rates thus should be as important as that of the 'global' forces associated with rifting and thermal subsidence.

Numerical model: fully coupled approach

Loads acting on the lithosphere can be subdivided into (Fig. 1): (1) positive loads (topography and deposited eroded material); (2) 'negative' loads due to erosion in the uplifted areas; (3) various subsurface loads including asthenospheric instability, thermal forces, crustal flow, regional forces; (4) restoring isostatic loads tending to compensate the loads 1–3. The lithospheric response depends on the mechanical properties of the lithosphere, which are partly controlled by its transient thermal state. Consequently, modelling of basin evolution requires a fully coupled approach accounting for surface processes, mechanical and thermal evolution of the system. All these factors are accounted for in the three-fold (surface processes, mechanical behaviour, heat transfer) numerical code Paravoz (Poliakov *et al.* 1993) based on the FLAC algorithm (Cundall 1989). Paravoz is a mixed finite-element/differences fully explicit time-marching Lagrangian scheme, a detailed explanation of which can be found in Cundall (1989). The Paravoz code can handle rheologically complex behaviours with large strains, including localization and propagation of non-predefined brittle shear bands, which simulate faults, power law creep and various kinds of strain softening and work hardening materials (examples of large-scale geodynamic applications can be found in: Burov & Molnar 1998; Gerbault *et al.* 1999; Burov & Guillou-Frottier 1999). For the purposes of the given study, we additionally modified the basic version of the code (Poliakov *et al.* 1993) to include: (a) the erosion/sedimentation model from (Burov & Cloetingh 1997); (b) the rheological and lithological model from Burov & Cloetingh (1997); (c) the heat advection and diffusion processes and initial temperature distribution model from Burov & Diament (1995).

Surface processes

The evolution of surface loads is described by transport and erosion laws derived from geomorphologic, stratigraphic and hydrologic observations (e.g. Carson & Kirkby 1972). The most commonly inferred models of surface processes include short-range erosion laws (parabolic diffusion equation) and fluvial transport laws (channel flow model) (Carson & Kirkby 1972; Gossman 1976; Kirkby 1986; Leeder 1991; Willgoose *et al.* 1991; Beaumont *et al.* 1992):

$$dh/dt = \nabla(k^*(x,y,h,\nabla h)\,\nabla h) \quad \text{(slope erosion by diffusion)} \tag{1}$$

$$q_{fe} = -K_r q_r \mathrm{d}h/\mathrm{d}l \ \text{(fluvial transport)} \tag{2}$$

where h is topography, t is time, x is horizontal coordinate, k^* is an experimentally adopted scale-dependent coefficient of erosion, which can be a function of coordinates x,y and of the local slope ∇h, q_r is river discharge, dh/dl is the slope in the

direction of the river drainage, K_r is a non-dimensional transport coefficient and l is the distance along the transporting channel. The use of the diffusion law for slope erosion is based on the observation that the erosion rates are not spatially constant but are strongly dependent on the local topography slopes because steeper slopes are more affected by gravity sliding, mechanical and climatic (e.g. wind) weathering. For 2D mechanical models described below, a 1D diffusion law is used:

$$dh/dt = k(x)\ (\partial h/\partial x)^n\ \partial^2 h/\partial x^2 = k^*\partial^2 h/\partial x^2 \qquad (3)$$

where $k(x)$ is a scale-dependent linear coefficient of erosion related to a generalized coefficient of erosion k^* as $k^* = k(x)(\partial h/\partial x)^n$. The parameter n can be equal to 0, 1, 2, 3. The case $n = 0$ is referred to as simple, linear, or zero-order erosion. The other cases are referred to as non-linear n-order erosion. The use of non-linear erosion laws is justified by the fact that not only the local erosion rates but also surface erodibility may be strongly slope dependent (e.g. steep slopes are more influenced by chemical alteration). Consequently, simple linear dependence of the erosion rate on the local slope assumed in linear diffusion equation may be not sufficient in the case of, for example, arid climatic environments, and stronger non-linear relations are needed. In particular, first-order non-linear erosion tends to form much less smoothed, sharpened topography features.

Rheology

Rheology and lithological structure are defined through yield-stress envelopes derived from rock mechanics data (e.g. Kirby & Kronenberg 1987; Kohlstedt *et al.* 1995). We use a non-linear brittle-elastic-ductile rheology for a granite-dominated upper crust, quartz-diorite or quartz-controlled lower crust, and olivine-dominated mantle. The ductile part obeys power law stress (σ) and exponential temperature (T) − stress/strain rate ($\dot{\epsilon}$) dependence:

$$\dot{\epsilon} = A^* \exp(-H^*/RT)\ (\sigma_1 - \sigma_3)^n, \qquad (4)$$

where σ_1 and σ_2 are the principal stresses, A^*, H^*, R, and n are the material constants explained in Table 1.

The brittle part follows Byerlee's law (Ranalli 1995), which is approximated by Mohr-Coulomb plasticity with friction angle 30° and cohesion of 20 MPa.

The elastic part is defined for commonly inferred values of Young's modulus and Poisson's ratio (Table 1; Turcotte & Schubert 1982).

Boundary and initial conditions

We used a constant extensional velocity as lateral boundary conditions at the both sides of the model, free surface as the upper boundary condition, and pliable Winkler (i.e. isostatic) basement as the bottom boundary condition. The rectangular numerical mesh is composed of quadruple elements (40000–125000), each constructed of two couples of overlapped triangular elements (Cundall 1989). The initial thermal structure is defined from the thermal age of the lithosphere at the time of rifting, calculated from the half-space cooling model (Burov & Diament 1995). A very small (100°C) Gaussian shape temperature anomaly at the base of the model is used for the initial perturbation needed to initiate rifting in the passive mode (e.g. Chery *et al.* 1992). The initial thickness of the upper and lower crustal layer is 20 km and 20 km, respectively (see Table 1). The total vertical and horizontal dimensions of the model vary, depending on the initial thermal structure, from 80 km × 20 km to 200 km × 150 km.

Experiments and results

We have conducted three sets of experiments employing major initial lithospheric structures conditioned by possible combinations of weak and strong rheological layers: the mechanical mantle layer can be (1) weaker than its crustal counterpart, or (2) stronger than it, or (3) equally competent. The ratio of the competence of the thickness of the mechanical mantle layer to that of the competent crustal layers is largely controlled by the geotherm (thermotectonic age, *ta*). Thus it is convenient to consider various lithospheric structures as a function of the lithospheric age. Three most representative cases may be envisaged: (1) a very young hot lithosphere with mechanically weak mantle part (thermotectonic age 50 Ma) - in this situation the thickness of the mechanical mantle does not exceed 10 km and crust plays a major role in the overall mechanical response of the lithosphere; (2) intermediate 'Jurassic' lithosphere (thermotectonic age 175 Ma) where the crust and mantle have approximately equal integrated rigidities; (3) cold lithosphere (thermotectonic age of 400 Ma) with thick mechanical mantle, which dominates the mechanical response.

The second scenario is of special interest for our study, since in this case weak ductile portions of the lower and intermediate crust can form flow channels delimited by rigid but highly flexible crustal and mantle layers.

For each set of experiments, we studied four basic situations: (1) slow extension (5 mm a^{-1}), no erosion; (2) slow extension, rapid erosion compara-

Table 1. *Values of parameters used*

Variable/parameter	Values and units	Comments
crustal thickness	40 km	continental crust
upper crustal thickness	20 km	continental crust
lower crustal thickness	20 km	continental crust
extension velocity	5, 10, 25 mm a^{-1}	background velocity on both sides
thermotectonic age, t_a	50, 250, 400 Ma	'young', 'intermediate', 'old' plate
coefficient of erosion k	0, 500, 1000 m^2 a^{-1}	zero, 'intermediate', 'rapid' erosion
background strain rate $\dot{\epsilon}$	s^{-1}, variable, 10^{-17} to 10^{-13} s^{-1}	obtained from calculations
Young's modulus E	80 GPa	all rocks
Poisson's ratio ν	0.25	all rocks
universal gas constant R	8.314 J mol^{-1} K^{-1}	used in power law
power law constant A_{c1}*	5×10^{-12} Pa^{-n} s^{-1}	wet granite (upper crust)
power law constant n_{c1}	3	wet granite (upper crust)
creep activation energy H^*_{c1}	190 kJ mol^{-1}	wet granite (upper crust)
power law constant A_{c2}*	5.01×10^{-15} Pa^{-n} s^{-1}	dry diorite (lower crust)
power law constant n_{c2}	2.4	dry diorite (lower crust)
creep activation energy H^*_{c2}	212 kJ mol^{-1}	dry diorite (lower crust)
power law constant A_m *	7×10^{-14} Pa^{-n} s^{-1}	olivine
power law constant n_m	3	olivine
creep activation energy H^*_m	520 kJ mol^{-1}	olivine
density ρ_s	2300 kg m^{-3}	uncompacted sediment
density ρ_{c1}	2650 kg m^{-3}	upper crust
density ρ_{c2}	2900 kg m^{-3}	lower crust
density ρ_m	3330 kg m^{-3}	lithospheric mantle
density ρ_a	3250 kg m^{-3}	asthenosphere
gravity constant g	9.8 m s^{-1}	
initial lithospheric thickness a_t	250 km	used to compute initial geotherms
temperature at the base of the lithosphere T_m	1330°C	used to compute initial geotherms
thermal diffusivity χ_{c1}	8.3×10^{-7} m^2 s^{-1}	upper crust
thermal diffusivity χ_{c2}	6.7×10^{-7} m^2 s^{-1}	lower crust
thermal diffusivity χ_m	8.75×10^{-7} m^2 s^{-1}	mantle lithosphere
thermal conductivity k_s	1.6 W m^{-1} K^{-1}	uncompacted sediment
thermal conductivity k_c1	2.5 W m^{-1} K^{-1}	upper crust
thermal conductivity k_{c2}	2 W m^{-1} K^{-1}	lower crust
thermal conductivity k_m	3.5 W m^{-1} K^{-1}	mantle lithosphere
radiogenic decay depth h_r	10 km	upper crust
surface heat production H_s	9.5×10^{-10} W kg^{-1}	upper crust

ble with the rock uplift/subsidence rate (that is k = 200–1000 m^2 a^{-1} for our experiments); (3) rapid extension (25 mm a^{-1}), no erosion; (4) rapid extension (25 mm a^{-1}), rapid erosion (500 m^2 a^{-1}).

The faults on the sides of the rift are not prexdefined but are initialized by the numerical code as a result of deformation. Hence, the fault distribution is one of the important outputs of the model, allowing for better constraints on the results of the experiments than in commonly inferred approaches. In particular, we studied the influence of the extension scenario and surface processes on fault localization, distribution and activity.

Case 1: young lithosphere, mantle weaker than crust

In this scenario, corresponding to *ta* = 50 Ma, the upper crustal layer is the only layer which can stay cold enough to preserve important strength. Consequently, this layer controls the strength and the mechanical response of the lithosphere. The necking level can be only very shallow in this case. The experiments with rapid extension (25 mm a^{-1} on both sides), in which the lithosphere was extended without and with concurrent erosion, produced quite different results (Fig. 2). In the case with no erosion the model-generated topography and faulted structures closely reproduce those of oceanic slow spreading zones (Buck & Poliakov 1998). This is expected, since there is little erosion at the sea bottom, and thus it is natural that the predicted structures are similar to those observed in the oceans. In the case of fast synrift erosion, the topography is highly different from the no-erosion case, not because it is smoothed by surface processes, but, importantly, the thickness and the entire deep structure of the rift also significantly

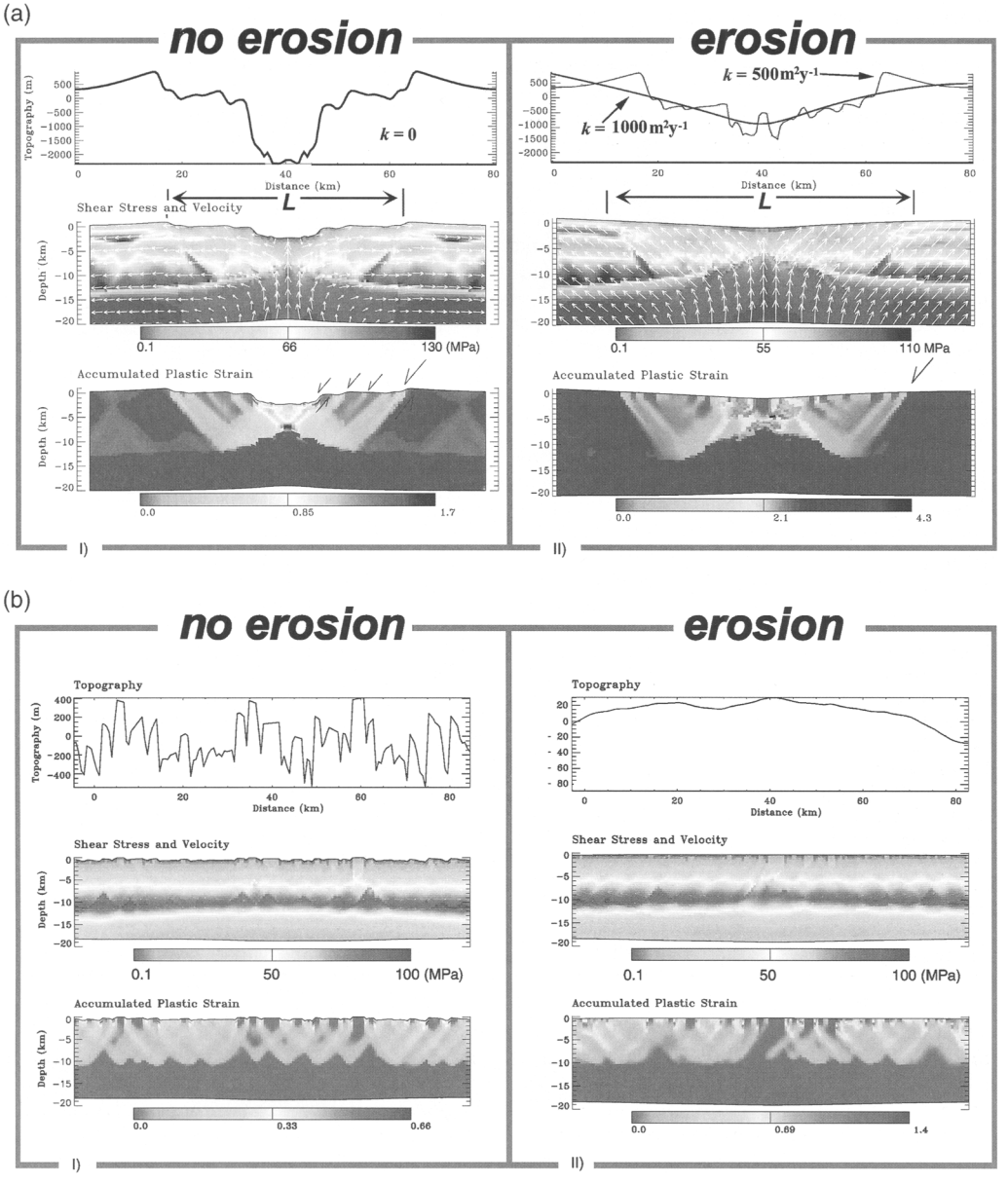

Fig. 2. Numerical modelling of synrift extension of a young lithosphere (age 50 Ma, upper crust dominates in the mechanical response): computed surface topography (top); shear stress and velocity vectors (middle); accumulated plastic strain (bottom). (**a**) The experiments shown in I and II are identical except that in case I there is no erosion, whereas in case II there is rapid erosion (k = 1000 m^2 a^{-1}). Also shown in (a) is surface topography for intermediate coefficient of erosion (k = 500 m^2 a^{-1}). One can see that erosion results in stronger thinning of the rift and produces a larger basin (according to the mechanism of Fig. 1) than in the case without erosion. (**b**) The same experiment as in (a) is represented, but for fast spreading lithosphere (50 mm a^{-1} on both sides). I shows the case without erosion, and II shows the case with rapid erosion (k = 1000 m^2 a^{-1}).

differ from the oceanic-like case: for the same boundary conditions, the rift became almost two times thinner at the centre and 1.5 times wider. Consequently, the β coefficient determined from subsidence curves using McKenzie's approach or from estimates of crustal thinning, will also be two times larger than in the first case. Yet, the amount of tectonic extension is the same in both cases. This effect of erosion is explained in Figure 1a: the erosion destroys the uppermost cold and strong crustal layer, which creates space for uplift of a weak ductile material and, consequently, results in faster localized thinning in the eroded areas. This effect would be amplified in case of the stress boundary conditions.

To test the model (compare our case with oceanic fast spreading zones), we have also conducted a fast extension experiment (50 mm a^{-1} on both sides), presented in Figure 2b. The structures resulting from the experiments without erosion strongly resemble those of oceanic zones of fast spreading. In the case with erosion, two times higher vertical acceleration of the crustal blocks can be also seen (compare the maximum strain rates in two cases).

Case 2: intermediate age lithosphere, mantle as strong as crust

This group of experiments relates to middle-aged lithospheric structure for which the mechanical thickness of the crust and mantle are approximately the same, and the lower crust is also strong enough to play a significant mechanical role. The upper, lower crust and competent mantle can be mechanically decoupled from each other by low strength ductile layers resulting from differences in creep activation temperatures specific for different crustal lithologies. Consequently, the mechanical behaviour of different layers becomes partly independent, and the equivalent elastic thickness of the system is much smaller than just the sum of the elastic thickness of each layer (Burov & Diament 1995), resulting in very 'weak' behaviour of the rift. This is certainly one of the most delicate cases since rift necking may occur simultaneously on different levels (Fig. 3), and the location of the maximum strain zone may switch from one depth level to another. Depending on the role of the surface processes as well as at which moment extension has ceased, the level of necking may be quite different, from very shallow to very deep. Erosion and sedimentation in the synrift stage may invert the direction of vertical crustal movement. Indeed, rapid erosional unloading, together with the lower crustal flow which it provokes, may cause a temporary uplift in the middle of the basin followed by a slow (with respect to thermal) subsidence. In the first case (no erosion), lower crustal flow also allows for relative uplift and subsidence of the upper crustal, lower crustal and mantle parts. Consequently, in this case the surface process may

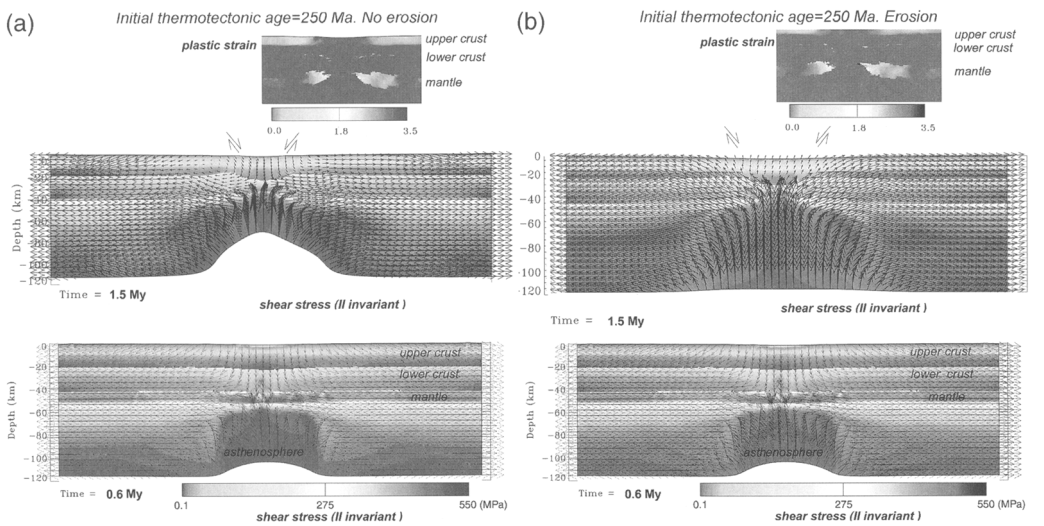

Fig. 3. Numerical model of synrift extension and erosion of a middle-aged lithosphere (250 Ma) with competent middle crustal and mantle layers (shear stress and velocity vectors). Subsidence and uplift are caused by interplay between sedimentary loading and mechanical response. (**a**) Experiments without erosion. (**b**) Experiments with intermediate erosion (k = 500 m^2 a^{-1}). For the developed stage, accumulated plastic strain ($\times$100%) in the central part of the rift is also shown in the top insert. The lower figure corresponds to 0.6 Ma since onset of rifting; the top figure corresponds to a developed rifting stage (1.5 Ma since onset of rifting).

not only accelerate or retard extension as in case 1, but also affect the level of necking resulting in different geometries of the rift basement and subsidence patterns.

During extension, some or all of the crustal and mantle rigid cores vanish in the centre of the rift being replaced by weak ductile or brittle zones. The rupture of the lower (intermediate) crustal core reduces its resistance to vertical uplift of the mantle layer. The latter rapidly ascends resulting in slower subsidence. In other cases, extension does not end in rupture, but in joining of the strong cores of the upper, lower crustal and mantle layers, resulting in flexural strengthening and in outward lateral expulsion of the ductile crust. This expulsion may lead to uplift on the rift flanks and crustal thickening outside of the basin. When the strong layers join each other under the basin forming a single 'neck', a mechanical coupling occurs, which leads to a step-like increase in the flexural thickness of the system (about two times; Burov & Diament 1995). The subsidence of the basin is thus instantly slowed down and is possibly followed by its lateral enlargement.

Mechanical coupling of competent layers below the basin is preceded by layer 'welding' under the rift flanks (Fig. 3), which locally doubles the elastic thickness in the flank area (Burov & Cloetingh 1997). The inelastic flexural yielding is also lowest under the flanks. This localized flexural border strengthening results in flexural uplift of the rift flanks and helps to maintain the flanks through the time. Indeed, gravity and apatite fission track studies of, for example, the East African rift system, indicate that continental lithosphere undergoing extension maintains considerable strength during the synrift stage, leading to long-lived rift flank uplift (Ebinger *et al.* 1989, 1991; Bechtel *et al.* 1990; van der Beek *et al.* 1995).

Since the mechanical strength and extension of the different strong layers may be quite different, at some stages one of the layers may deflect much more strongly than the others, creating additional space under the basin. This space may be filled by the ductile crust from outside of the basin, delaying subsidence or even uplifting the centre of the basin. As was pointed out by Kaufman & Royden (1994), the crustal and mantle lithosphere may have highly different β coefficients. Here we show that necking may occur on different levels in the crust and in the mantle, so that the internal crustal levels may also exhibit quite different coefficients of extension and even deflect in opposite directions. For example, the upper crust may subside while the lower or intermediate crust moves upward. Since the competent core of the upper crustal layer may be quite thin (a few kilometres), it follows that upper crustal subsidence or uplift may be significantly affected by normal loads generated by surface processes.

Finally, in the post-rift stages, our experiments confirm the semi-analytical model of Burov & Cloetingh (1997) who have shown that the surface processes and induced crustal flow may enhance basin subsidence. In addition to their model, another effect is revealed by the numerical experiments: the presence of a low viscosity lower or intermediate crustal layer may result in detachment from the mantle lithosphere, and also lead to slowed subsidence at the surface, since subsidence (due to cooling) of the deep mantle layers may have no immediate effect at the surface. Thus the mantle may subside separately, with the mantle-crust 'gap' being filled by rapid lower crustal flow.

Case 3: old lithosphere, mantle stronger than crust

In this part of the experiments the strong mantle layer was considerably thicker than the strong crustal layers, conditioned by a cold (400 Ma) geotherm. In this case (Fig. 4), there is no significant crust-mantle decoupling and flow, and crustal deformation is controlled by the mantle lithosphere. Yet, even in the case of very strong lithosphere, the surface processes remain important. Erosion and sedimentation can provoke quiescence and even uplift periods during the synrift phase, and favour development of asymmetric extension patterns by amplifying local anomalies in surface uplift rate.

Discussion: coupling between surface and subsurface processes

Evolution of topography and crust

The topography produced by our coupled model is geologically realistic compared to common geological and gydynamic hypotheses, e.g. rift structures and fault distributions (Salvenson 1978). Major stages of rift development and fault evolution were reproduced (Fig. 5), such as half-graben, graben, continental extensional basins, and oceanic basins.

Influence of the erosion law

The isostatic uplift of the rift shoulders in response to erosion is an important mechanism for maintaining a relatively high rate of material flux from hillslopes. However, erosion of the drainage divides on the top of the rift shoulders results in their retreat from the centre of the basin. At the same time the sedimentary wedge migrates towards the

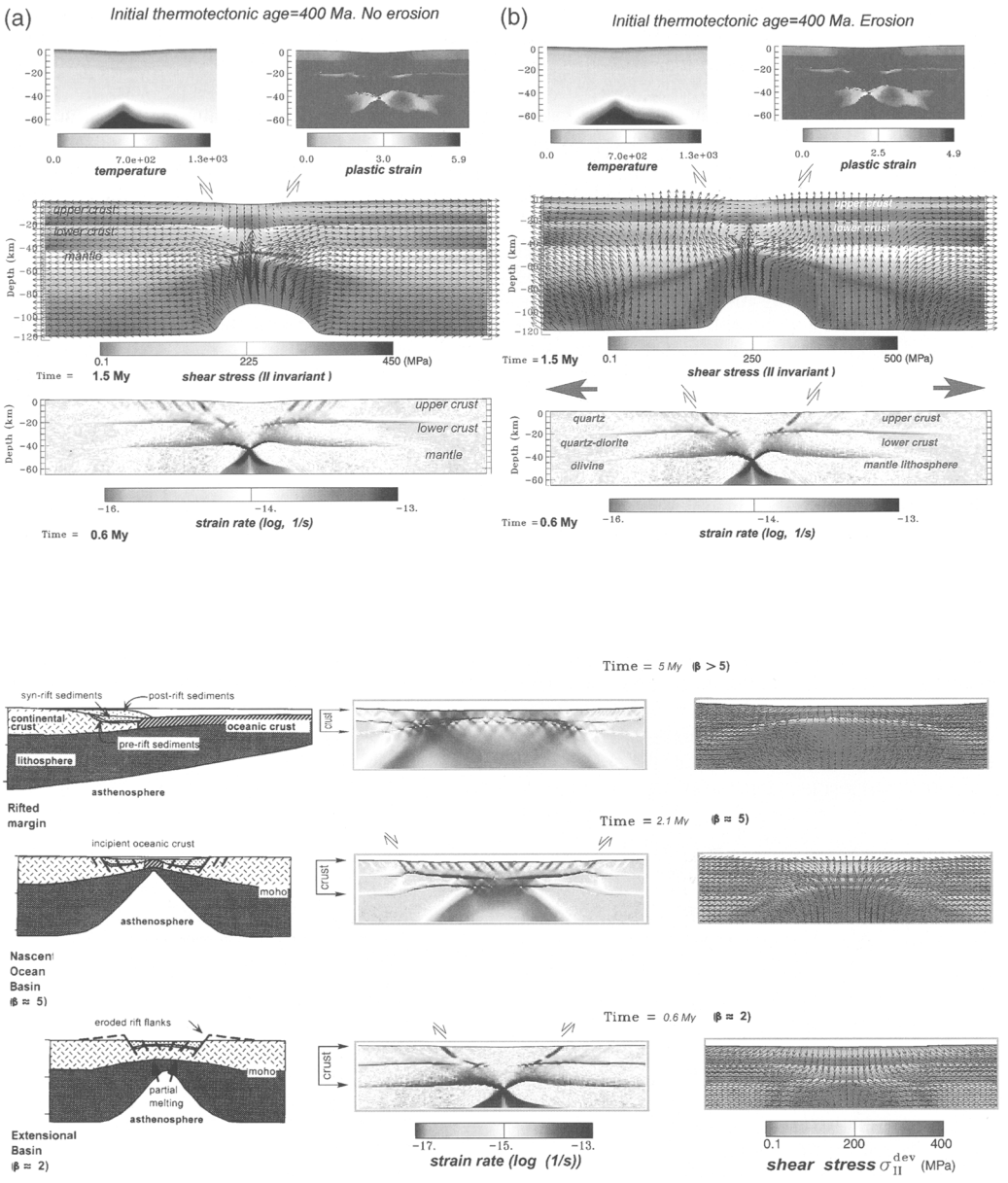
(a)
Initial thermotectonic age=400 Ma. No erosion
(b)
Initial thermotectonic age=400 Ma. Erosion
temperature
plastic strain
upper crust
lower crust
mantle
Depth (km)
Time = 1.5 My
shear stress (II invariant)
0.1
225
450 (MPa)
500 (MPa)
strain rate (log, 1/s)
Time = 0.6 My
quartz
quartz-diorite
olivine
mantle lithosphere
Time = 5 My (β > 5)
syn-rift sediments
post-rift sediments
continental crust
oceanic crust
pre-rift sediments
lithosphere
asthenosphere
Rifted margin
Time = 2.1 My (β ≈ 5)
incipient oceanic crust
moho
Nascent Ocean Basin (β ≈ 5)
Time = 0.6 My (β ≈ 2)
eroded rift flanks
partial melting
Extensional Basin (β ≈ 2)
crust
strain rate (log (1/s))
shear stress σ_{II}^{dev} (MPa)

The major effect is that it tends to keep the hillslopes steeper than in the linear erosion case (Fig. 4). Thus it favours more localization of the rift shoulders than the conventional erosion law. The relief produced by the non-linear erosion is also more realistic than the relief produced by linear erosion.

When erosion is low, basin subsidence is retarded. The related pressure gradient might not be sufficient to counteract the pressure gradients due to density contrasts between the crust and mantle beneath the rift shoulders. The net flux in the lower crust can be reversed in this case (Figs 3 & 4). It will thus retard subsidence of the basin and accelerate collapse of the rift shoulders (Fig. 6).

Post-rift extension and compression

The accumulation of the eroded matter also requires an adequate increase of the basin volume in time. This can occur both in the vertical and horizontal directions, by an increase of the depth of the basin due to subsidence but also by progressive horizontal spreading and onlap of sedimentary deposits. A logical effect of the latter process is widening of the basin resulting in additional extension. This gravity-driven extension is facilitated by secondary post-rift extension due to diverging flow in the lower crust.

Erosion cannot respond immediately to changes in surface uplift, particularly because it is conditioned by a number of independent factors such as climate and surface erodibility. Also, rock viscosity limits the rate of the response of the lower crust and asthenosphere to alternations in surface load. This naturally introduces some delay in the feedback between the surface and subsurface processes. As is known from general studies of feedback systems (e.g. cybernetics, theory of automation, theory of oscillators, operations research theory, etc.), positive feedback with no or in-phase time shift with respect to the input signal results in amplification of the system reply, and the system can be even made to resonate. Out-of-phase (e.g. delayed positive feedback) may result in various oscillations on the output of the system, especially in cases of rapid changes on the input or in the behaviour of the feedback itself. For this reason, one can expect extensional and compressional oscillations, as well as oscillations in the rate of subsidence caused by transient imbalances between the forces of the gravity collapse, lower crustal flow and erosion. Such oscillations in the rate of basin subsidence are indeed observed is several cases (e.g. Dnieper-Donez basin). Though they can probably be explained by eustatic changes or deep mantle processes, the 'feedback' nature is not excluded. Such oscillations were also demonstrated in previous semi-analytical orogenic models (Avouac & Burov 1996), as well as in the numerical experiments of the present study. Even though

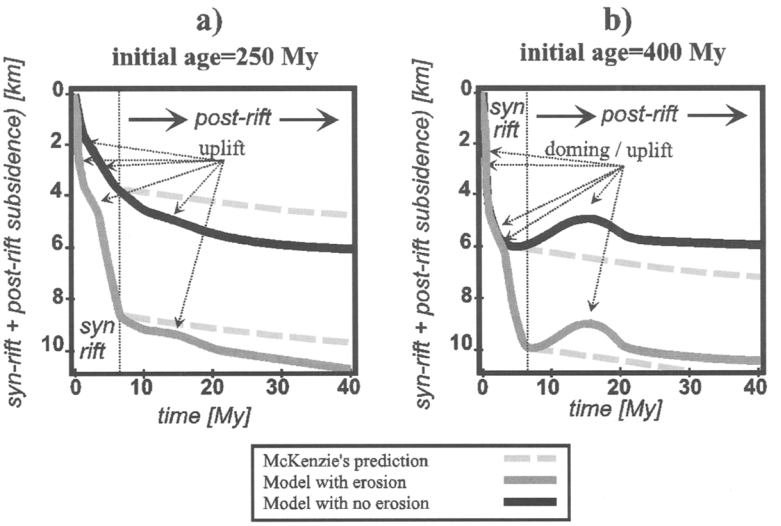

Fig. 6. Subsidence curves corresponding to the case of Figure 3 compared to the classic McKenzie (1978) model. (**a**) Subsidence curves for thermotectonic age 250 Ma. (**b**) Subsidence curves for thermotectonic age 400 Ma. Grey dashed lines show predictions for respective McKenzie models. Note periods of relative syn- and post-rifting uplifts related to structural changes (disappearance of certain mechanical layers) and misbalances between the surface processes and tectonic reaction.

we are confident that these oscillations are not numerical artifacts (their period ranges from 10 ka to several hundred thousand years, which is much longer than the period of possible artificial oscillations due to propagation of numerical waves (<0.1 ka), this topic itself definitely requires a separate detailed study.

Conclusions

Erosion and sedimentation enhance rift thinning and stabilize uplift on the rift shoulders, even during the synrift phase, which is the result of the present study, and largely during the post-rift phase (here the numerical results confirm the analytical predictions made by Burov & Cloetingh 1997). The role of surface processes in the synrift phase is especially important for rifts with young and middle-age thermal structure, where it can result in increase by a factor of 2 or more in extension than without synrift erosion. This has very important consequences for most common stratigraphic evolution models based upon McKenzie's (1978) or Royden & Keen's (1980) method of estimation of the coefficients of extension.

This study shows that the syn- and post-rift evolution of a rift is to a large extent a result of coupling between surface processes (erosion and sedimentation) and response of the lithosphere that includes both rebound effects of localized weakening due to load, and flow in the lower crust. In confirmation of the previous simplified studies (e.g. Burov & Cloetingh 1997), we conclude that flow in the lower crust facilitates both subsidence and crustal thinning, uplift of the rift shoulders and variation in the width of the basin (secondary extension). If either erosion or subsidence terminates for some reason, the lower crustal flow will facilitate collapse of rift shoulders and thickening of the crust and uplift of the basin. Erosion and sedimentation in the post-rift phase can be responsible for delays and accelerations of subsidence with respect to common kinematic/thermal models. It is evident that the carrying capacity and preferential direction of the fluvial network largely control timing of sedimentary filling of the basin (e.g. Kooi & Beaumont 1994). The tectonic reaction to morphological loading and unloading depends on the viscosity and other thermomechanical parameters of the system. Consequently, important delays may appear between the tectonic action (subsidence) and morphological reaction (surface processes). In our case this results in uplift and subsidence events without apparent reason.

We have demonstrated that synrift and post-rift subsidence may occur at a slower rate than inferred from common models (20–25%), and can be characterized by sufficiently long periods of stagnation or uplift resulting from interplay between different rheological layers, lower or intermediate crustal flow and surface processes. Rupture of the quasi-elastic core of the intermediate crustal level may result in rapid uplift of the mantle layer. Joining ('welding together') of the rigid layers followed by expulsion of the ductile crust results in temporal flexural strengthening, stagnation of subsidence and widening of the basin. In the post-rift phase, multiple periods of stagnation result from interplay between surface processes and the mechanical response of the lithosphere. This model explains most of the actively discussed deviations from thermal subsidence models such as slow or rapid subsidence, periodical stagnations, and uplifts.

The model explains basin evolution patterns using only relatively well-constrained internal crustal structure, and observable surface processes as boundary/initial conditions. It does not need to invoke external, poorly constrained phenomena such as phase transitions or the inversion of tectonic stresses.

Surface processes and interplay between various mechanical layers in the lithosphere result in different levels of necking for the same initial structure and boundary conditions. In different stages of extension, the level of necking may switch from deep to shallow and vice versa. Thus, depending on the duration of the tectonic extension, the basin starts its post-rift subsidence from a shallow or deep level of necking. Consequently, the traditionally estimated level of necking cannot be directly used to infer the initial lithospheric structure or subsidence.

Evolution of the surface load in time due to sedimentation in the hinterland and erosion in higher flank areas continuously changes the strength of the underlying lithosphere. Because flexure and inelastic effects significantly change the geometry of the crust and Moho, and especially the level of necking, it appears that it is difficult to trust in estimates of the β-factors made on the basis of observations of crustal geometry or backstripping reconstructions. We have demonstrated that the presence of low viscosity lower crust of laterally variable thickness may introduce an important time-dependent contribution to the mechanical response of the lithosphere. This effect must be taken into account not only in basin modelling, but also in models of post-glacial rebound of the lithosphere used to determine the effective viscosity of the asthenosphere. One can predict some extensional and compressional oscillations, as well as oscillations in the rate of subsidence caused by transient imbalances between the forces of the gravity collapse, lower crustal flow and erosion.

In contrast to previous studies (e.g. England

1983; Dunbar & Sawyer 1988), and in confirmation of some qualitative analytical results obtained in (Burov & Cloetingh 1997; Burov & Poliakov 2001), we show that post-rift strengthening results in greater integrated strength in the middle of the rift basin than immediately outside its flanks. The rift flank areas stay weak because they are permanently locally weakened by flexure and by enhanced conductive (in the lithosphere) and also convective (in the asthenosphere) heat transport on the borders of the extended area. If extension continues, these areas nucleate new rifting (not to be mixed with the results of Lavier *et al.* (2000) on short distance normal fault jumping in extending ideal brittle layer). This secondary rifting does not require any new far-field extension episode, because self-stressing due to the gravity spreading and induced flows in the ductile crust and the asthenosphere is already sufficient. Interplays between strengthening and extension at the end of a long (e.g. longer than 5 Ma) synrift phase or at the beginning of a post-rift phase may explain so-called abandoned rifts.

We greatly benefited from the highly instructive and detailed review provided by the first anonymous reviewer and T. den Bezemer. A co-creator of Paravoz, Y. Podladchikov, is deeply thanked for generously sharing his knowledge and experience. We also benefited from discussions with C. Ebinger, S. Cloetingh, M.-P. Doin, P. Van der Beek and J. Chery. This study is supported by IT Program of INSU (CNRS).

Appendix

Numerical model and rheological assumptions

For numerical experiments (Fig. 1b) we adopted the code Paravoz (Poliakov *et al.* 1993), which allows for mixed brittle, elastic, viscous and non-Newtonian temperature, stress and strain rate-dependent power-law rheology and complex geometrical structures. This code belongs to the so-called Fast Lagrangian Analysis of Continua family (FLAC) (Cundall 1989) of large strain, fully explicit time-marching numerical algorithms based on a Lagrangian 'moving grid' method. It is not clear whether FLAC codes should belong to finite difference or to finite element methods, since they use a mixed formulation, which includes an explicit method to solve algebraic finite-difference equations, but implicit, matrix-oriented solution schemes used in finite element methods. As in finite element methods, the FLAC method uses arbitrarily shaped numerical elements. To allow small strain solutions to work for large strains, FLAC codes rely on very small time steps. They solve for near incremental strains and then explicitly numerically integrate them, because the result of the model is by default the cumulative effect of all the small strains over all time steps.

The major advantage of the FLAC method is its capacity to model initialization and evolution of non-predefined faults, which is crucial for this study. This algorithm and its application to caldera modelling were described in detail in Burov & Guillou-Frottier (1999).

As with other FLAC codes, Paravoz solves Newton's equations of motion in continuum mechanics formulation:

$$\rho \partial v_i/\partial t - \partial \sigma_{ij}/\partial x_j - \rho g_i = 0 \qquad \text{(A1)}$$

where v is velocity, g is the acceleration due to gravity and ρ is the density. The numerical mesh moves with the material, and at each time step the new positions of the mesh grid nodes are calculated from the current velocity field (Cundall 1989). As mentioned, the code is explicit and uses very short time steps and very small elements. Since no global stiffness matrix is needed, it is a trivial matter to update coordinates at each time step in large-strain mode. Equation (A1) is solved in the local evolving coordinates, thus the strain can be small with respect to moving Lagrangian coordinates, but large with respect to a fixed Cartesian grid. The local area rotation at large strain is accounted for by adjusting appropriate tensor components, e.g. stress tensor components σ_{ij} are adjusted as $\sigma_{ij} = \sigma_{ij} + (\omega_{ik}\sigma_{kj} - \sigma_{ik}\omega_{kj})$ where the finite rotation ω is given by $\omega_{ij} = \frac{1}{2}(\partial u_j/\partial x_j - \partial u_j/\partial x_i)$. Solution for velocities at mesh points is used to calculate element strains ϵ_{ij}. These strains are employed in the constitutive relations yielding element stresses σ_{ij} and equivalent forces $\rho \partial v_i/\partial_t$, which provide input for the next calculation cycle. For elastic and brittle materials the constitutive relations have a linear form:

$$\epsilon_{ij} = A\sigma_{ij} + A_0 \qquad \text{(A2)}$$

where A, A_0 are constitutive parameters (Table 1). For a ductile rheology these relations become:

$$\dot{\epsilon}_{ij} = A\sigma^{n-1}\sigma_{ij} \qquad \text{(A3)}$$

where $\dot{\epsilon}_{ij}$ is the strain rate and $\sigma = (\frac{1}{2}\sigma_{ij}\sigma_{ij})^{\frac{1}{2}}$ is the effective stress (second invariant of the deviatoric stress). The variables n (the effective stress exponent) and A (constitutive parameter) describe the properties of a specific material (Table 1). For ductile materials, n usually equals 2–4 and A is depth and temperature dependent ($A = A_0 \exp(-H/RT)$). For the brittle and elastic materials A is usually only depth dependent. Yet, A and A_0

can be functions of strain or stress for softening or hardening materials. To allow for explicit solution of the governing equations, the FLAC method employs a dynamic relaxation technique based on introduction of artificial inertial masses in the dynamic system. The adaptive remeshing technique allows strain localizations resulting in the formation of faults. The method does not use inherent rheology assumptions, in contrast with common finite-element techniques.

For the elastic rheology, we use the following constitutive parameters: E (Young's) modulus = 80 GPa and ν (Poisson's ratio) = 0.25. The brittle behaviour is presented by Mohr-Coulomb plasticity with cohesion softening (friction angle 30°, cohesion decreases from 20 MPa at zero strain to 0 at 1% strain; Gerbault *et al.* 1998).

Since the ductile rheology is temperature dependent, the mechanical balance equations are coupled with the heat transport equations:

$$div(\mathbf{k}\nabla T) - \rho C_p \partial T/\partial t + H_r = \mathbf{v}\nabla T \qquad \text{(A4)}$$

where $\mathbf{v}$ is the velocity tensor, C_p is the specific heat, $\mathbf{k}$ is the thermal conductivity tensor, H is radiogenic heat production per unit volume (here we use the commonly inferred values adopted, e.g. in Burov & Diament (1995). The solution of the right-hand side (diffusive) and left-hand side (advective) part of Equation A4 is separated: the latter is calculated automatically when solving the equations of motion, whereas the former is computed using a separate procedure.

The size of the mesh elements was between 50 m × 50 m and 250 m × 250 m.

References

AVOUAC, J. P. & BUROV, E. B. 1996. Erosion as a driving mechanism of intracontinental mountain growth. *Journal of Geophysical Research,* **101**, 17747–17769.

BASSI, G. 1995. Relative importance of strain rate and rheology for the mode of continental extension. *Geophysical Journal International,* **122**, 195–210.

BEAUMONT, C., FULLSACK, P. & HAMILTON, J. 1992. Erosional control of active compressional orogens. *In:* MCCLAY, K. R. (ed.) *Thrust Tectonics.* Chapman & Hall, London, 1–31.

BECHTEL, D., FORSYTH, D. W., SHARPTON, V. L. & GRIEVE, R. A. F. 1990. Variations in effective elastic thickness of the North American lithosphere. *Nature,* **343**, 636–638.

BRAUN, J. & BEAUMONT, C. 1989. A physical explanation of the relation between flank uplifts and the breakup unconformity at rifted continental margins. *Geology,* **17**, 760–765.

BUCK, W. R. 1991. Modes of continental lithospheric extension. *Journal of Geophysical Research,* **96**, 20161–20178.

BUCK, W. R. & POLIAKOV, A. N. B. 1998. Abyssal hills formed by stretching oceanic lithosphere. *Nature,* **392**, 272–275.

BUROV, E. B. & CLOETINGH, S. 1997. Erosion and rift dynamics: new thermomechanical aspects of post-rift evolution of extensional basins. *Earth and Planetary Science Letters,* **150**, 7–26.

BUROV, E. B. & DIAMENT, M. 1995. The effective elastic thickness (Te) of continental lithosphere: What does it really mean? *Journal of Geophysical Research,* **100**, 3905–3927.

BUROV, E. B. & GUILLOU-FROTTIER, L. 1999. Thermomechanical behavior of large ash-flow calderas, *Journal of Geophysical Research,* **104(10)**, 23081–23109.

BUROV E. B. & MOLNAR, P. 1998. Gravity anomalies over the Ferghana Valley (central Asia) and intracontinental Deformation. *Journal of Geophysical Research,* **103**, 18137–18152.

BUROV, E. B. & POLIAKOV, A. N. B. 2001. Erosion and rheology controls on synrift and postrift evolution: Verifying old and new ideas using a fully coupled numerical model. *Journal of Geophysical Research,* **106**, 16461–16481.

CARSON, M. A. & KIRKBY, M. J. 1972. *Hillslope Form and Processes.* Cambridge University Press, Cambridge.

CHÉRY, J., LUCAZEAU, F., DAIGNIERES, M. & VILOTTE, J.-P. 1992. Large uplift of rift flanks: A genetic link with lithospheric rigidity? *Earth and Planetary Science Letters,* **112**, 195–211.

CLOETINGH, S. & BUROV, E. B. 1996. Thermomechanical structure of European lithosphere: constraints from rheological profiles and EET estimates. *Geophysical Journal International,* **124**, 695–723.

CLOETINGH, S. A. P. L., WORTEL, M. J. R. & VLAAR, N. J. 1982. Evolution of passive continental margins and initiation of subduction zones. *Nature,* **297**, 139–142.

CUNDALL, P. A. 1989. Numerical experiments on localization in frictional materials. *Ingenieur-Archiv,* **59**, 148–159.

DUNBAR, J. A. & SAWYER, D. S. 1988. Continental rifting at pre-existing lithospheric weakness. *Nature,* **333**, 450–452.

EBINGER, C. J., BECHTEL, T. D., FORSYTH, D. W. & BOWIN, C. O. 1989. Effective elastic plate thickness beneath the East African and Afar Plateaux and dynamic compensation of the uplifts. *Journal of Geophysical Research,* **94**, 2883–2901.

EBINGER, C. J., KARNER, G. D. & WEISSEL, G. D. 1991. Mechanical strength of extended continental lithosphere: constraints from the western rift system, Africa. *Tectonics,* **10**, 1239–1256.

EBINGER, C., JACKSON, J., FOSTER, A. & HAYWARD, N. 1999. Extensional basin geometry and the elastic lithosphere. *Philosophical Transactions of the Royal Society of London,* **A357**, 741–762.

ENGLAND, P. 1983. Constraints on extension of the continental lithosphere. *Journal of Geophysical Research,* **88**, 1145–1152.

ENGLAND, P. & RICHARDSON, S. W. 1980. Erosion and the age dependence of the continental heat flow. *Geophysical Journal of the Royal Astronomical Society,* **62**, 421–437.

GERBAULT, M., POLIAKOV, A. N. B. & DAIGNIERES, M.

1998. Prediction of faulting from the theories of elasticity and plasticity; what are the limits? *Journal of Structural Geology,* **20**, 301–320.

GERBAULT, M., BUROV, E. B., POLIAKOV A. & DAGNIERES, M. 1999. Do faults trigger folding in the lithosphere? *Geophysical Research Letters,* **26(2)**, 271–274.

GOSSMAN, H. 1976. Slope modelling with changing boundary conditions – effects of climate and lithology. *Zeitschrift fr Geomorphologie N.F.*, Suppl. Bd. **25**, 72–88.

HOPPER, J. R. & BUCK, W. R. 1996. The effect of lower crustal flow on continental extension and passive margin formation. *Journal of Geophysical Research,* **101**, 20175–20194.

KAUFMAN, P. S. & ROYDEN, L. H. 1994. Lower crustal flow in an extensional setting: Constraints from the Halloran Hills region, eastern Mojave Desert, California. *Journal of Geophysical Research,* **99**, 15723–15739.

KIRBY, S. H. & KRONENBERG, A. K. 1987. Rheology of the lithosphere: selected topics. *Review of Geophysics,* **25**, 1219–1244.

KIRKBY, M. J. 1986. A two-dimensional model for slope and stream evolution. *In*: ABRAHAMS, A. D. (ed.) *Hillslope Processes*. Allen and Unwin, Boston, 203–224.

KOHLSTEDT, D. L., EVANS, B. & MACKWELL, S. J. 1995. Strength of the lithosphere: Constraints imposed by laboratory experiments. *Journal of Geophysical Research,* **100**, 17587–17602.

KOOI, H. & BEAUMONT, C. 1994. Escarpment evolution on high-elevation rifted margins: insights derived from a surface processes model that combines diffusion, advection and reaction. *Journal of Geophysical Research,* **99**, 12191–12210.

KUSZNIR, N. & KARNER, G. 1985. Dependence of the flexural rigidity of the continental lithosphere on rheology and temperature. *Nature,* **316**, 138–142.

KUSZNIR, N. J. 1991. The distribution of stress with depth in the lithosphere: thermo-rheological and geodynamic constraints, *Philosophical Transactions of the Royal Society of London,* **A337**, 95–110.

LAVIER, L. L., BUCK, W. R. & POLIAKOV, A. N. B. 2000. Factors controlling normal fault offset in ideal brittle layer. *Journal of Geophysical Research,* **105**, 23431–23442.

LEEDER, M. R. 1991. Denudation, vertical crustal movements and sedimentary basin infill. *Geologische Rundschau,* **80**(2), 441–458.

LOBKOVSKY, L. I. & KERCHMAN, V. I. 1992. A two-level concept of plate tectonics: application to geodynamics. *Tectonophysics,* **199**, 343–374.

MCKENZIE, D. 1978. Some remarks on the development of sedimentary basins. *Earth and Planetary Science Letters,* **40**, 25–32.

POLIAKOV A. N. B., PODLADCHIKOV, Y. & TALBOT, C. 1993. Initiation of salt diapirs with frictional overburden: numerical experiments. *Tectonophysics,* **228**, 199–210.

POLIAKOV, A. N. B., PODLADCHIKOV, Y. Y. & YUEN, D. A. (in press). A model of sedimentary basin formation with phase-transition and erosion: explanation of syn-rift uplift and stratigraphic onlap. *Tectonophysics.*

RANALLI, G. 1995. *Rheology of the Earth* (second edition). Chapman & Hall, London.

ROHRMAN, M., VAN DER BEEK, P., ANDRIESSEN, P. & CLOETINGH, S. 1995. Meso-Cenozoic morphotectonic evolution of southern Norway: Neogene domal uplift inferred from apatite fission track thermochronology. *Tectonics,* **14**, 704–718.

ROYDEN, L. & KEEN, C. E. 1980. Rifting process and thermal evolution of the continental margin of Eastern Canada determined from subsidence curves, *Earth and Planetary Science Letters,* **51**, 343–361.

SALVENSON, J. O. 1978. Variations in the geology of rift basins; a tectonic model. *Conference Proceedings Los Alamos Scientific Laboratory,* **7487**, 82–86.

STEPHENSON, R. A., NAKIBOGLU, S. M. & KELLY, M. A. 1989. Effects of astenosphere melting, regional thermoisostasy, and sediment loading on the thermomechanical subsidence of extensional sedimentary basins. *In*: PRICE, R. A. (ed.) *Origin and Evolution of Sedimentary Basins and their Energy and Mineral Resources.* American Geophysical Union, Washington, Geophysical Monographs, **48**, 17–27.

TURCOTTE, D. L. & SCHUBERT, G. 1982. *Geodynamics. Applications of Continuum Physics to Geological Problems.* Wiley, New York.

VAN BALEN, R., VAN DER BEEK, P. A. & CLOETINGH, S. A. P. L. 1995. The effect of rift shoulder erosion on stratal patterns at passive margins: Implications for sequence stratigraphy. *Earth and Planetary Science Letters,* **134**, 527–544.

VAN DER BEEK, P., ANDRIESSEN, P. & CLOETINGH, S. 1995. Morphotectonic evolution of rifted continental margins; inferences from a coupled tectonic-surface processes model and fission-track thermochronology. *Tectonics,* **14**, 406–421.

WATTS, A. B. & TORNE, M. 1992. Crustal structure and the mechanical properties of extended continental lithosphere in the Valencia through (western Mediterranean). *Journal of the Geological Society, London,* **149**, 813–827.

WHITE, N. & MCKENZIE, D. P. 1988. Formation of the "Steer's Head" geometry of sedimentary basins by differential stretching of the crust and mantle. *Geology,* **16**, 250–253.

WILLGOOSE, G., BRAS, R. L. & RODRIGUES-ITURBE, I. 1991. A coupled channel network growth and hillslope evolution model 1. Theory. *Water Research,* **27**, 1671–1684.